

Received December 27, 2020, accepted January 6, 2021, date of publication January 11, 2021, date of current version January 20, 2021.

Digital Object Identifier 10.1109/ACCESS.2021.3050409

# The Eco-Driving Considering Coordinated Control Strategy for the Intelligent Electric Vehicles

LIANG HAO<sup>1,2</sup>, BOHUA SUN<sup>3,4</sup>, GANG LI<sup>2</sup>, AND LIXIN GUO<sup>1</sup>

<sup>1</sup>School of Mechanical Engineering and Automation, Automotive Engineering, Northeastern University, Shenyang 110819, China

<sup>2</sup>Automobile and Traffic Engineering College, Liaoning University of Technology, Jinzhou 121001, China

<sup>3</sup>State Key Laboratory of Automotive Simulation and Control, Jilin University, Changchun 130025, China

<sup>4</sup>Borch Future Automotive Technologies Ltd., Changchun 130025, China

Corresponding author: Bohua Sun (450772088@qq.com)

This work was supported in part by the China (CHN) Department National Natural Science Foundation Project under Grant 51675257, and in part by the Serving Local Projects of Liaoning Province Education Department under Grant JFL201915402.

**ABSTRACT** Minimum energy consumption with maximum comfort driving experience defines the ideal human mobility. Recent technological advances in most highly automated driving systems on electric vehicles with regenerative braking system not only enhance the safety and comfort level but also present a significant opportunity for automated eco-driving. This research focuses on the longitudinal eco-driving considering the coordinated control for 4WD intelligent electric vehicles. The intelligent electric vehicle framework with 4-wheel hub motors is established and the intention-aware longitudinal automated driving strategy for overall traffic situation levels is proposed. Further, the coordinated control strategy arbitrates the control mode basing on the traffic situation level and distributes braking forces between the electronic hydraulic braking system and the cooperative regenerative auxiliary braking system. The proposed strategy is verified in the co-simulation environment and field test respectively. Test results show optimal control effects in overall traffic situation levels and an enhanced energy recycling efficiency.


**INDEX TERMS** Intelligent electric vehicle (IEV), coordinated control, NMPC, intention-aware, object perception.

## I. INTRODUCTION

Consumption of unrenewable fuels and critical pollution, such as global warming, unexpected climate changes and unprecedented amounts of air pollution, have caused both energy and environmental issues [1]. They strengthen the significance of the efforts toward the development of clean energy vehicles to a sustainable level [2]. Meanwhile, with respect to many previous studies on intelligent vehicles which tend to oversimplify or even ignore the co-driving technology with the vehicle-traffic interaction, the intention-aware integrated driving strategy for overall traffic situation levels has attracted much recent attention from all over the world [3], [4]. To satisfy these demands, electrification and intelligence technologies are key development tendencies to future vehicles [5]. Intelligent Electric Vehicles (IEVs), the automated driving vehicles with clean energy, should

achieve a holistic control integration among driving safety, comfort and sustainable energy.

As a highly integrated product consisting of electrification, informatization and intelligence, IEVs offer unprecedented opportunities for automated safe and energy-efficient driving, which can be called eco-driving, and the dynamic interaction and synergy among individual subsystems in IEVs need to be analyzed and modeled [6], [7]. On the other hand, how to integrate the energy optimization during the longitudinal eco-driving process and vehicle safety under complex scenarios with uncertainties is a formidable challenge. To overcome this problem, the traffic situation should be estimated in real time and an intention-aware longitudinal automated driving strategy applicable to overall traffic situation levels needs to be established [8]. Moreover, the coordinated control of the control mode basing on the traffic situation level and braking forces between the electronic hydraulic braking system and the cooperative regenerative braking system needs to be tackled [9], [10]. In summary, our main contributions are listed as follows:

The associate editor coordinating the review of this manuscript and approving it for publication was Kan Liu .

- An intensive intelligent electric vehicle framework basing on the optimal mechanism of information flow, energy flow and substance flow is established.
- An intention-aware longitudinal automated driving strategy applicable to overall traffic situation levels is proposed for the eco-driving strategy.
- A coordinated control strategy is proposed to arbitrate control modes and distribute braking forces for the eco-driving strategy.
- The proposed eco-driving strategy is verified in the co-simulation environment and field test respectively.

The remainder of this article is organized as follows. In Section II, an overview of the intelligent electric vehicles is discussed. Section III introduces the 4WD intelligent electric vehicle framework. Section IV focuses the longitudinal automated driving strategy and section V proposes the coordinated control strategy. In section VI, co-simulation environment and field test are conducted and performance results are shown and discussed. Finally, key conclusions and related future works are presented in section.

## II. RELATED WORK

Related work about IEVs focuses on the vehicle framework considering physical states and dynamic characteristics of key assemble models, longitudinal auto-driving strategies in various kinds of traffic situation levels and the coordinated control strategy between the electronic hydraulic braking system and the cooperative regenerative braking system. Technical details are introduced and analyzed as follows.

### A. INTELLIGENT ELECTRIC VEHICLES

The dynamic motion process of IEVs reflects the dynamic interaction and cooperation among substance flow, energy flow and information flow [11]. The power for IEVs' motion is embodied as the energy flow, the dynamic process of energy conversion, consumption and recovery [12]. Flow and transfer characteristics of energy flow is established as the physical models of motor and battery [13]. The change of vehicle states represented by kinematics and compliance has typical characteristics of substance flow and controlled by the vehicle dynamic control system [14]. The substance flow based evolution process of IEVs' movement focuses on the path-following and aims at a subtle control effect [15]. IEVs' perception and decision-making capability basing on Multi-source sensing fusion conducts as the information flow and constitutes the automated system [16]. Automated controllers receive multi-modal sensing information to perceive static and dynamic traffic participants [17]. The collaborative optimization of energy flow, substance flow and information flow is the fundamental solution to achieve driving safety, comfort and sustainable energy for IEVs and should be given more attention [18]. An integration framework for IEVs basing on the optimal mechanism of information flow, energy flow and substance flow is absent and needs to be established

as the dynamic vehicle system foundation for the coordinated control framework and control strategy.

### B. LONGITUDINAL AUTOMATED DRIVING STRATEGY

As the main function of IEVs, longitudinal automated driving framework consists of the adaptive cruise control in normal scenarios and obstacle avoidance in emergency scenarios [19]. Typical cruise control models for normal scenarios have been built considering car-following features and driving styles with comprehensive parameters [14]. In succession with the physical models, data-driven based adaptive cruise control models by integrating communication technologies have been proposed to achieve cooperative cruise functions [20]. In emergency scenarios, automatic emergency braking systems with accuracy braking performs are developed to guarantee driving safety [21]. However, traffic uncertainties involving vehicle motion intentions are always ignored and traffic situation levels should be evaluated to switch among control modes as well [22]. An accurate motion intention estimation has a significant effect on improving the decision-making capability for IEVs [23], [24]. The data-driven intention identification method has achieved a high accuracy but should the acceptable potential in the traffic situation assessment should be improved for longitudinal automated driving [25], [26]. Therefore, an intention-aware longitudinal automated driving strategy applicable to overall traffic situation levels should be established to overcome scenario uncertainties and improve driving safety.

### C. COORDINATED CONTROL STRATEGY FOR IEVs

Coordinated control strategy for IEVs mainly consists of switching mechanism among a variety of driver assistance systems, such as forward collision warning, adaptive cruise control and automatic emergency braking, and the braking force distribution mechanism between the electronic hydraulic braking system and the cooperative regenerative braking system [27], [28]. A reasonable and smooth switching mechanism among driver assistance systems plays a positive role in improving driving safety and comfort [29]. The driving risk assessment based switching mechanism achieves the pass rates above 90% in some typical scenarios [30]. Meanwhile, the braking force distribution mechanism can realize the regenerative and hydraulic braking simultaneously [31]. The dynamic response characteristics of in-wheel motors and hydraulic response characteristics need to be compensated in different braking stage and regenerative braking energy should be recycled to the maximum extent [32], [33]. The braking torque of the lower-level distribution controller is used to compensate for the insufficient braking torque to realize a smooth transition between the braking modes [34]. Key parameters in the braking force distribution strategy, such as the optimal distribution coefficients, need to be achieved by the genetic algorithm and weight coefficients can be used to achieve a dynamic distribution [35]. What's more, intervention mechanisms of the upper-level controller, such as the driver assistance controller

or the active safety controller, need to be developed [36], [37]. Taken the above mentioned into consideration, A coordinated control strategy should be developed to arbitrate control modes and distribute braking forces for the eco-driving strategy.

### III. 4WD INTELLIGENT ELECTRIC VEHICLE FRAMEWORK

#### A. THE INTEGRATED IEV FRAMEWORK

A distributed hub-motor 4WD IEV configuration basing on the optimal mechanism of Information Flow (IF), Energy Flow (EF) and Substance Flow (SF) is proposed as shown in Figure 1 and its corresponding architecture of eco-driving is shown in Figure 2. Multi-modal sensing data from intelligent sensors, such as lidar, radar and camera, and vehicle state sensors, such as the Wheel Speed Sensor (WSS) the Inertial Navigator Unit (INU) and Tire Pressure Sensor (TPS), are used to perceive the human-vehicle-scenario situation, and perception results are fed into the decision-making module. Multi-modal sensing data, the perception process, decision-making logic and their flow characteristics constitute the IF. I-booster controlled by the Hydraulic Control Unit (HCU), hub motors for Motors and Generators (M/G) controlled by the Motor Control Unit (MCU), battery packs controlled by the Battery Management System (BMS) and their Energy Management System (EMS) are embodied as EF. Automated strategies controlled by the Vehicle Control Unit (VCU) and Intelligent Control Unit (ICU) represent the change in vehicle states and can be described as SF. The IEV achieves driving tasks basing on the collaborative optimization of IF, EF and SF and its multi-scale and multi-level optimization model

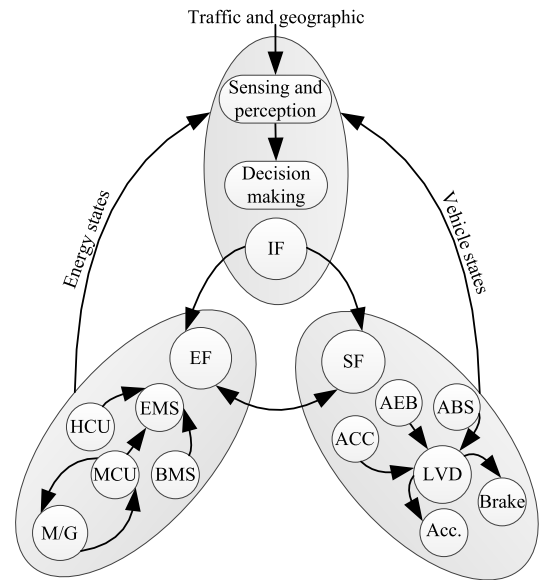


FIGURE 2. The integrated IEV framework basing on energy flow, substance flow and information flow.

should be established. Therefore, key subsystem models of IEVs are proposed and verified in the next section.

#### B. KEY SUBSYSTEM MODELING OF IEVS

The 26-freedom vehicle dynamic model in Carsim2016<sup>®</sup> is proposed to describe kinematic and dynamic characteristics for the IEV's SF. The hub motor in EF is proposed as the Permanent Magnet Synchronous Motor (PMSM) and its equivalent circuit model is shown in Figure 3.

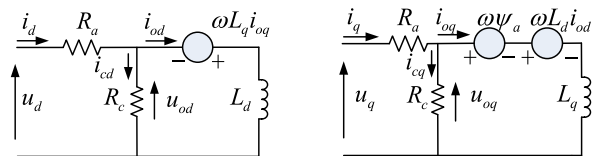


FIGURE 3. The PMSM model for hub motors considering iron loss.

The voltage equation considering iron loss for the hub motor when it's served as the motor in the steady condition is expressed as follows.

$$\begin{bmatrix} u_d \\ u_q \end{bmatrix} = R_a \begin{bmatrix} i_{od} \\ i_{oq} \end{bmatrix} + \left(1 + \frac{R_a}{R_c}\right) \begin{bmatrix} u_{od} \\ u_{oq} \end{bmatrix} \quad (1)$$

$$\begin{bmatrix} u_{od} \\ u_{oq} \end{bmatrix} = \begin{bmatrix} 0 & -\omega L_q \\ \omega L_d & 0 \end{bmatrix} \begin{bmatrix} i_{od} \\ i_{oq} \end{bmatrix} + \begin{bmatrix} 0 \\ \omega \psi_a \end{bmatrix} \quad (2)$$

$$\begin{bmatrix} i_{od} \\ i_{oq} \\ i_{cd} \\ i_{cq} \\ \omega \end{bmatrix} = \begin{bmatrix} i_d - i_{cd} \\ i_q - i_{cq} \\ \frac{\omega L_q i_{oq}}{R_c} \\ \frac{R_c (\psi_a + L_d i_{od})}{\omega} \\ p\omega_m \end{bmatrix} \quad (3)$$

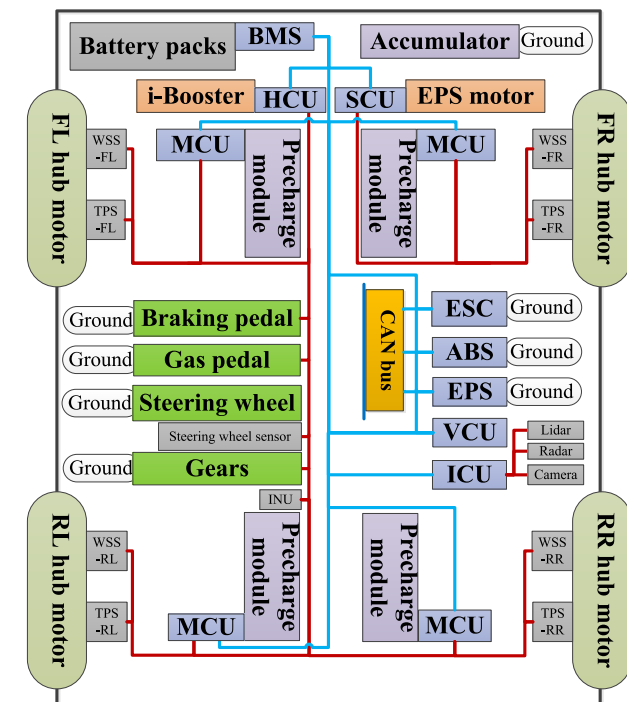


FIGURE 1. The IEV's configuration.

where  $u_d$  and  $u_q$  are stator's voltages in  $d$  and  $q$  axis,  $i_d$  and  $i_q$  are stator currents in  $d$  and  $q$  axis,  $L_d$  and  $L_q$  are equivalent inductances in  $d$  and  $q$  axis,  $\psi_a$  is the chain amplitude of the permanent magnet,  $R_a$  is the stator equivalent resistance,  $\omega$  and  $\omega_m$  are the electrical and mechanical angular speeds and  $p$  is the number of pole pairs.

The external characteristics when the hub motor is served as the generator is shown in Figure 4.

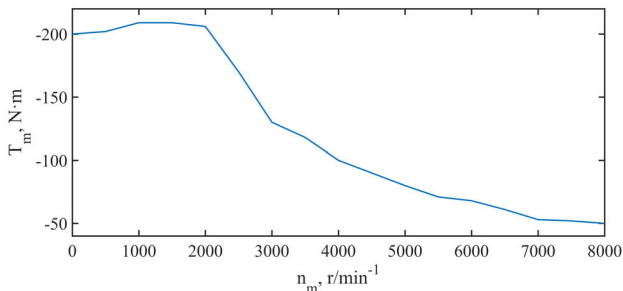


FIGURE 4. The generator's external characteristic.

As the key subsystem in IF, lidar is modeled considering its generic detection function and signal attenuation feature. The geometric model describes the detection function of object positions and orientations and can be implemented by utilizing geometric methods in [38]. The signal attenuation model reveals the phenomenon that the effective detection range of a lidar varies with the laser transmission media and can be expressed as followed.

$$R_{dmax}^2 = A_L \rho_s \exp(-2\gamma R_{dmax}) \quad (4)$$

$$A_L = \frac{P_T \pi D^2 \eta_s}{16 P_{Rmin}}, \quad \gamma = \frac{\ln\left(\frac{R_1^2 \rho_2}{R_2^2 \rho_1}\right)}{2(R_2 - R_1)} \quad (5)$$

where  $R_{dmax}$  is the maximum detection range,  $A_L$  is the system constant,  $\rho_s$  is the surface reflectivity of laser beam,  $\gamma$  is the atmosphere attenuation coefficient impacted by atmospheric molecules and aerosol in different weather conditions,  $P_T$  is laser's transmission power,  $D$  is the aperture diameter,  $\eta_s$  is the system efficiency,  $P_{Rmin}$  is laser's minimum return power,  $(R_1, R_2)$  is two typical objects of  $R_{dmax}$  and  $(\rho_1, \rho_2)$  is the corresponding reflectivity.

The lidar model is compared with the measured curve and its accuracy is shown in Figure 5 where a high fitting degree with the lidar specification is obtained.

#### IV. LONGITUDINAL AUTOMATED DRIVING STRATEGY

The hierarchical strategy for longitudinal automated driving is as shown in Figure 6. Human-vehicle-scenario status and motion intentions of surrounding vehicles are obtained in the traffic situation assessment. Traffic situation is predicted and the controller corresponding to the desired driving mode is chosen. Taken the economy, comfort, safety and following performances into consideration, the optimum effect for eco-driving is conducted.

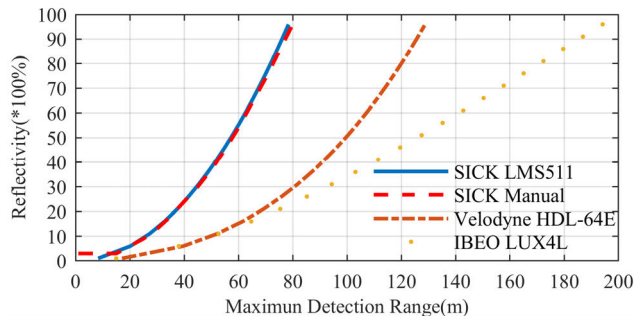


FIGURE 5. Relationship between maximum detection range and reflectivity.

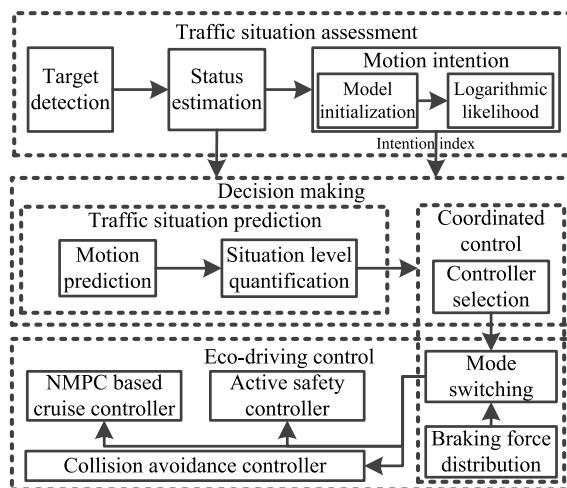


FIGURE 6. Framework of the longitudinal automated driving strategy.

#### A. THE INTENTION-AWARE BASED TRAFFIC SITUATION ASSESSMENT

Traffic situation assessment provides the IEV with the status detection and motion intentions of traffic participants. As the perception foundation, ground segmentation and grid maps are built. Point clouds from the lidar contain both the ground object information and need to be classified and cut out. The Region of Interest (ROI) is defined as a rectangle region with  $\pm 20m$  lateral width and  $\pm 40m$  longitudinal length and random sample consensus algorithm is utilized to fit plane geometric model. Therefore, ground point clouds are labeled as inliers and object point clouds on the road are labeled as outliers in Figure 7.

Grid maps are used to represent scenarios with obstacle point clouds and consist of  $400 \times 200$  grids basing on the grid resolution of 0.2m. Elements in each grid are the normalized height calculated by the height gap between the highest and the lowest points and target detection are conducted basing on image processing algorithm. Hough transform is used to further detect sidewalks, and vehicle objects on the road are collected. Given the L-shape and particular size of vehicles in grid maps, domain connecting detection algorithm is utilized.

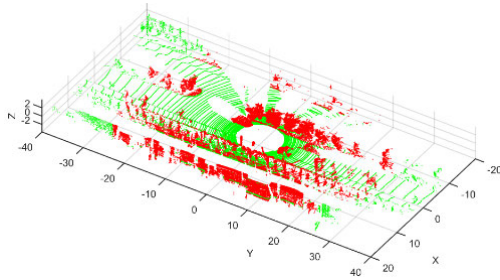


FIGURE 7. Road segmentation results.



FIGURE 8. Road grid map calculated by height gap.

Targets are fitted as rectangles and their positions, sizes and orientations are calculated.

Basing on the surrounding vehicle detection, same targets are associated and their motion states are tracked with the Kalman filter [39]. States of being evaluated are as follows.

$$x_{KF} = [P_{olon}, v_{olon}, a_{olon}, P_{olat}, v_{olat}, a_{olat}, \varphi, \dot{\varphi}] \quad (6)$$

where  $P_o = [P_{olon}, P_{olat}]$ ,  $v_e = [v_{olon}, v_{olat}]$  and  $a_c = [a_{olon}, a_{olat}]$  are the position, velocity and acceleration of the target and  $\varphi$  is the heading angle. The state transform matrix  $A_{KF}$  can be defined as a constant acceleration model and be expressed with the updating time step  $T_{KF}$  as followed.

$$A_{KF} = \begin{bmatrix} 1 & T_{KF} & 0.5T_{KF}^2 & 0 & 0 & 0 & 0 & 0 \\ 0 & 1 & T_{KF} & 0 & 0 & 0 & 0 & 0 \\ 0 & 0 & 1 & 0 & 0 & 0 & 0 & 0 \\ 0 & 0 & 0 & 1 & T_{KF} & 0.5T_{KF}^2 & 0 & 0 \\ 0 & 0 & 0 & 0 & 1 & T_{KF} & 0 & 0 \\ 0 & 0 & 0 & 0 & 0 & 1 & 0 & 0 \\ 0 & 0 & 0 & 0 & 0 & 0 & 1 & T_{KF} \\ 0 & 0 & 0 & 0 & 0 & 0 & 0 & 0 \end{bmatrix} \quad (7)$$

The observation states are positions and orientation of the critical target and can be defined as the observation matrix.

$$H_{KF} = \begin{bmatrix} 1 & 0 & 0 & 0 & 0 & 0 & 0 & 0 \\ 0 & 0 & 0 & 1 & 0 & 0 & 0 & 0 \\ 0 & 0 & 0 & 0 & 0 & 0 & 1 & 0 \end{bmatrix} \quad (8)$$

The process noise covariance  $Q_{KF}$  and the disturbance transformation matrix  $\Gamma$  are expressed as follows.

$$Q_{KF} = \Gamma^T Q_N \Gamma \quad (9)$$

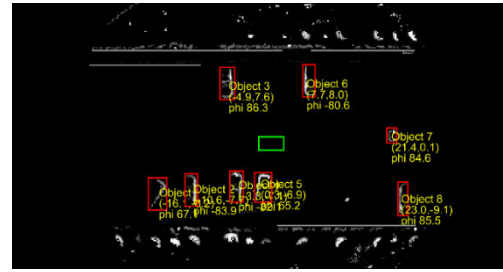


FIGURE 9. Target detection example.

$$\Gamma = \begin{bmatrix} \frac{T_{KF}^3}{6} & \frac{T_{KF}^2}{2} & T_{KF} & 0 & 0 & 0 & 0 & 0 \\ 0 & 0 & 0 & \frac{T_{KF}^3}{6} & \frac{T_{KF}^2}{2} & T_{KF} & 0 & 0 \\ 0 & 0 & 0 & 0 & 0 & 0 & \frac{T_{KF}^2}{2} & T_{KF} \end{bmatrix} \quad (10)$$

$$Q_N = \begin{bmatrix} \sigma_{alon}^2 & 0 & 0 \\ 0 & \sigma_{alat}^2 & 0 \\ 0 & 0 & \sigma_{dp}^2 \end{bmatrix}, \quad R_{KF} = \begin{bmatrix} \sigma_{lon}^2 & 0 & 0 \\ 0 & \sigma_{lat}^2 & 0 \\ 0 & 0 & \sigma_p^2 \end{bmatrix} \quad (11)$$

where  $\sigma_{alon}$ ,  $\sigma_{alat}$  and  $\sigma_{dp}$  are the standard deviations of the longitudinal acceleration disturbance, lateral acceleration disturbance and heading angle rate,  $\sigma_{lon}$ ,  $\sigma_{lat}$  and  $\sigma_p$  are the measurement error standard deviations of the longitudinal, lateral and heading angle, and  $R_{KF}$  is the measurement noise covariance.

Given that eco-driving is of short duration and high identification accuracy, the motion intention index  $I_m$  of IEV's adjacent vehicles is basing on the Reactive Motion Intention Model (RMIM) and the non-adjacent ones is basing on the Driving Motion Intention Model (DMIM). The status  $s_0$  and relative states  $ds_0$  of surrounding vehicles are a series of continuous observable sequences in the time domain and affect the internal states of the adjacent moment, then the first-order Multi-dimension Gaussian Hidden Markov Process (MGHMP) is proposed for the identification of motion intentions as shown in Figure 10.

$$I_m = \{I_R, I_D\} = \{f_R(s_0, ds_0), f_D(s_0)\} \quad (12)$$

$$I_R = \{I_{FA}, I_{HT}, I_{NM}, I_{CI}\}, I_D = \{I_{LE}, I_{RI}, I_{FO}\} \quad (13)$$

where  $I_R$  is the intention index of the RMIM and  $I_D$  is that of the DMIM,  $I_{FA}$ ,  $I_{HT}$ ,  $I_{NM}$  and  $I_{CI}$  are intentions of staying away, hesitating, maintaining and approaching respectively, and  $I_{LE}$ ,  $I_{RI}$  and  $I_{FO}$  are intentions of turning left, turning right and keeping forward respectively.

Hidden state set  $q_t$  with  $N$  dimensions and  $\kappa$  possible observations constitutes MGHMP and the initial states  $\zeta$  are distributed as follows.

$$\zeta = \{\zeta_i, \zeta_i = P[q_1 = i], 1 \leq i \leq N\} \quad (14)$$



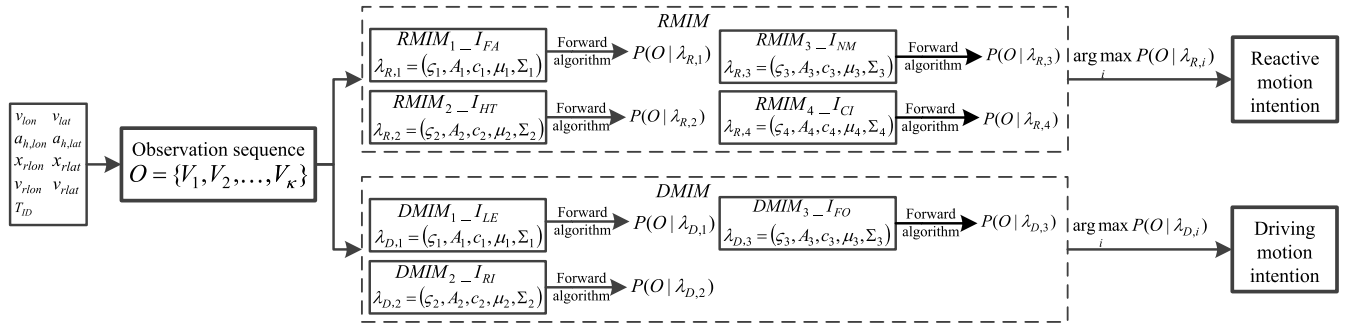


FIGURE 10. The identification framework for traffic situation assessment.

The process of  $q_t$  transition is defined as the probability matrix  $A$ .

$$A = \{a_{ij}, a_{ij} = P[q_{t+1} = j | q_t = i], 1 \leq i, j \leq N\} \quad (15)$$

The observable sequence set  $O$  and the corresponding observation probability density function  $B$  are as followed.

$$O = \{V_i, i = 1, \dots, \kappa\} \quad (16)$$

$$B = \left\{ b_j(O), b_j(O) = \sum_{k=1}^M c_{jk} N(O | \mu_{jk}, \Sigma_{jk}), 1 \leq j \leq N \right\} \quad (17)$$

$$\sum_{k=1}^M c_{jk} = 1, \int b_j(O) dO = 1, c_{jk} \geq 0, 1 \leq j \leq N, 1 \leq k \leq M \quad (18)$$

where  $V$  is the possible observation and  $\kappa$  is the number of  $V_i$ ,  $c_{jk}$  is the  $k^{th}$  mixed weighting coefficient in  $j^{th}$  state and  $M$  is the Gaussian mixture number.  $N(O | \mu_{jk}, \Sigma_{jk})$  is the Gaussian probability density function with mean  $\mu$  and covariance  $\Sigma$ .

The traffic situation is assessed basing on the combination of RMIM and DMIM those are defined by a tuple  $\lambda$  with  $N$  states. Motion intention probabilities are defined as the logarithmic likelihood and the maximum one in each model is the corresponding type of the motion intention.

$$\lambda = (\zeta, A, c, \mu, \Sigma) \quad (19)$$

$$\text{Loglik}(\theta) = \ln [P(O | \lambda)] \quad (20)$$

### B. SITUATION PREDICTION BASED SITUATION LEVEL ESTIMATION

The IEV focuses on the collision avoidance in emergency scenarios and the situation level estimation basing on the situation prediction is proposed for all situation levels. The traffic situation prediction aims at predicting threat as shown in Figure 11 and two steps are conducted. The first step is calculating the Time-To-Collision (TTC) and the second step is to decide threat level based on TTC.

The prediction based method with TTC is adaptive to various scenarios. Future trajectories of both the IEV and

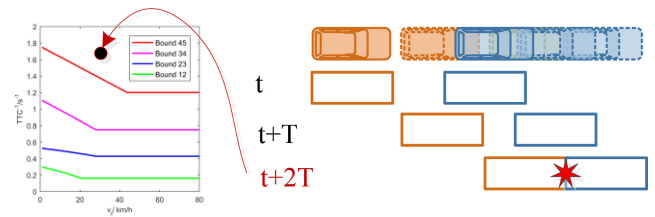


FIGURE 11. Traffic situation prediction process.

the surrounding vehicles are predicted basing on the constant acceleration model and collision detection conducts on all predicted steps to confirm the collision moment.

$$\begin{bmatrix} P_{oi,t+1} \\ v_{ei,t+1} \\ a_{ci,t+1} \end{bmatrix} = \begin{bmatrix} 1 & \chi & 0.5\chi^2 \\ 0 & 1 & \chi \\ 0 & 0 & 1 \end{bmatrix} \begin{bmatrix} P_{oi,t} \\ v_{ei,t} \\ a_{ci,t} \end{bmatrix} + \begin{bmatrix} 0.5\chi^2 \\ \chi \\ 1 \end{bmatrix} \omega_a \quad (21)$$

where  $\chi$  is the time step and  $\omega_a$  is the standard deviation of the minor white noise.

Potential collisions at each  $\chi$  are abstracted as rectangles basing on the separating axis theorem [40]. TTC corresponds to the collision moment and the threat level set  $\Phi$  is decided by an experimental method based on the reverse TTC.

$$\Phi = \left\{ \begin{array}{l} 1 = \text{safety, } 2 = \text{warning, } 3 = \text{emergency warning,} \\ 4 = \text{light interference, } 5 = \text{emergency interference} \end{array} \right\} \quad (22)$$

Boundaries between adjacent threat levels varies with the velocity  $v_c$  km/h of the critical target vehicle as follows.

$$\begin{cases} TTC_{4 \leftrightarrow 5}^{-1} = \max [(1.7609 - 0.0128v_c), 1.20] \\ TTC_{3 \leftrightarrow 4}^{-1} = \max [(1.1184 - 0.0131v_c), 0.75] \\ TTC_{2 \leftrightarrow 3}^{-1} = [\max [(1.1184 - 0.0131v_c), 0.75] + 1.00]^{-1} \\ TTC_{1 \leftrightarrow 2}^{-1} = [\max [(0.4760 - 0.0134v_c), 0.20] + 1.22]^{-1} \end{cases} \quad (23)$$

### C. NMPC BASED ECO-DRIVING DRIVING STRATEGY

The IEV drives in the cruise mode in normal scenarios and a Nonlinear Model Prediction Control (NMPC) is proposed for the adaptive cruise control. A dynamic car-following internal

model and the optimum braking force distribution strategy in section V are developed. The response characteristics of hub motors and the hydraulic braking system to the desired acceleration is approximated as a discrete first-order system.

$$a_{h,lon}(k + 1) = (1 - \frac{T_s}{\tau})a_{h,lon}(k) + \frac{T_s}{\tau} \cdot \xi \cdot a_u(k) \quad (24)$$

where  $\xi$  is the system gain,  $\tau$  is the time constant,  $a_u$  is the desired acceleration and  $a_h$  is the actual acceleration. Then the car-following internal model is discretized as followed.

$$\begin{cases} x(k + 1) = \alpha \cdot x(k) + \beta \cdot a_u(k) + G \cdot \omega(k) \\ x(k) = [x_{rlon}(k), v_{rlon}(k), v_{lon}(k), a_{h,lon}(k), j_{lon}(k)] \end{cases} \quad (25)$$

$$\alpha = \begin{pmatrix} 1 & T_s & 0 & -\frac{T_s^2}{2} & 0 \\ 0 & 1 & 0 & -T_s & 0 \\ 0 & 0 & 1 & T_s & 0 \\ 0 & 0 & 0 & 1 - \frac{T_s}{\tau} & 0 \\ 0 & 0 & 0 & -\frac{1}{\tau} & 0 \end{pmatrix}, \quad \beta = \begin{pmatrix} 0 \\ 0 \\ 0 \\ \frac{T_s \cdot \xi}{\tau} \\ \frac{1}{\tau} \end{pmatrix}, \quad G = \begin{pmatrix} \frac{T_s^2}{2} \\ \frac{T_s}{2} \\ 0 \\ 0 \\ 0 \end{pmatrix} \quad (26)$$

where  $x_{rlon}$  and  $v_{rlon}$  are the longitudinal relative distance and relative velocity,  $v_{lon}$ ,  $a_{h,lon}$  and  $j_{lon}$  are IEV's longitudinal velocity, acceleration and jerk respectively.

Basing on the integrated IEV framework. optimization performance indexes are established for the eco-driving in normal scenarios. The economy indicator basing on the EF quantifies the recovery energy  $L_{eco}$  in the prediction interval and the recovery energy  $E_m$  in prediction time  $k$  is derived as (18) and shown in Figure 12.

$$E_m(a_{h,lon}(k), v_{lon}(k)) = \min(F_{reg}(a_{h,lon}(k)), F_{Bmax}(v_{lon}(k))) \cdot (v_{lon}(k) \cdot T_s + \frac{1}{2} a_{h,lon}(k) \cdot T_s^2) \quad (27)$$

where  $F_{reg}$  is the total regenerative brake force and  $F_{Bmax}$  is the maximum regenerative braking torque at the given  $v_{lon}(k)$ .

Therefore,  $L_{eco}$  is expressed as follows.

$$L_{eco} = Q_1 \sum_{k=1}^p E_m(a_{h,lon}(k), v_{lon}(k)) \quad (28)$$

The comfort, following and safety indicators are basing on both IF and SF. The comfort indicators can be represented by the  $a_{h,lon}$  and  $j_{lon}$  [41]. The higher fitting degree the eco-driving strategy matches with the driving style, the more comfort drivers will feel. Then the comfort indicator  $c_{omf}$  in prediction time  $k$  and  $C_{omf}$  in the prediction interval are expressed as follows.

$$c_{omf}(k) = Q_2 \cdot (a_{h,lon}(k) - a_{ham}(k))^2$$

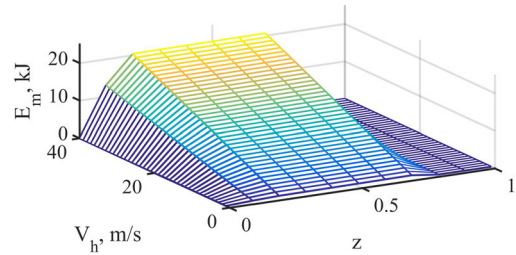


FIGURE 12. The relationship among regenerative energy, speed and braking strength.

$$+ Q_3 \cdot (j_{lon}(k) - j_{ham}(k))^2 + Q_4 \cdot a_u^2(k) \quad (29)$$

$$C_{omf}(k) = \sum_{k=1}^p c_{omf}(k) \quad (30)$$

where  $a_{ham}(k)$  and  $j_{ham}(k)$  are the prediction result based on the driving style model in [10],  $Q_2$ ,  $Q_3$  and  $Q_4$  are weight coefficients.

The following indicator specifies following performances of velocity and safety workshop distance and the following indicator  $l_t$  in time  $k$  and  $L_t$  in prediction interval are listed.

$$l_t(k) = Q_5 \cdot \delta^2(k) + Q_6 \cdot v_{rlon}^2 \quad (31)$$

$$L_t(k) = \sum_{k=1}^p l_t(k) \quad (32)$$

where  $\delta$  is the distance following error,  $Q_5$  and  $Q_6$  are weight coefficients.

The safety indicator constraints the  $x_{rlon}$  to avoid collision and can be expressed as follows.

$$d_c \leq x_{rlon}(k) \leq d_{max} \quad (33)$$

where  $d_c$  is the minimum safe distance.

Taken above performance indicators into consideration, constraints in NMPC can be expressed as follows.

$$M \leq L \cdot x(k) \leq N \quad (34)$$

$$M = \begin{pmatrix} d_c \\ v_{min} \\ a_{min} \\ j_{min} \end{pmatrix}, \quad L = \begin{pmatrix} 1 & 0 & 0 & 0 & 0 \\ 0 & 0 & 1 & 0 & 0 \\ 0 & 0 & 0 & 1 & 0 \\ 0 & 0 & 0 & 0 & 1 \end{pmatrix}, \quad N = \begin{pmatrix} d_{max} \\ v_{max} \\ a_{max} \\ j_{max} \end{pmatrix} \quad (35)$$

Supposing  $a_{h,lon}$  keeps the same in  $p$  steps and IEV's states from  $k^{th}$  to  $(k + p)^{th}$  step time can be predicted as follows.

$$\hat{X}_p(k + p|k) = \bar{\alpha} \cdot x(k) + \bar{\beta} \cdot U(k + m) + \bar{G} \cdot W(k + p) \quad (36)$$

$$\hat{X}_p(k + p|k) = \begin{pmatrix} \hat{x}_p(k + 1|k) \\ \hat{x}_p(k + 2|k) \\ \vdots \\ \hat{x}_p(k + p|k) \end{pmatrix},$$

$$U(k+m) = \begin{pmatrix} a_u(k) \\ a_u(k+1) \\ \vdots \\ a_u(k+m-1) \end{pmatrix}$$

$$W(k+p) = \begin{pmatrix} a_l(k) \\ a_l(k+1) \\ \vdots \\ a_l(k+p-1) \end{pmatrix} = \begin{pmatrix} a_l(k) \\ a_l(k) \\ \vdots \\ a_l(k) \end{pmatrix} \quad (37)$$

$$\bar{\alpha} = \begin{pmatrix} \alpha \\ \alpha^2 \\ \vdots \\ \alpha^p \end{pmatrix},$$

$$\bar{\beta} = \begin{pmatrix} \beta & 0 & \dots & 0 \\ \alpha\beta & \beta & \ddots & \vdots \\ \vdots & \vdots & \ddots & 0 \\ \alpha^{p-1}\beta & \alpha^{p-2}\beta & \dots & \alpha^{p-m}\beta \end{pmatrix}$$

$$\bar{G} = \begin{pmatrix} G & 0 & \dots & 0 \\ \alpha G & G & \ddots & \vdots \\ \vdots & \vdots & \ddots & 0 \\ \alpha^{p-1}G & \alpha^{p-2}G & \dots & G \end{pmatrix} \quad (38)$$

where  $a_l(k)$  is the  $a_{h,lon}$  in the  $k^{th}$  time step. Constraints in  $p$  prediction steps are derived as follows.

$$\bar{M} \leq \bar{L} \cdot \hat{X}_p(k+p) \leq \bar{N}$$

$$U(k+m) \leq U_{max}$$

$$-U(k+m) \leq -U_{min} \quad (39)$$

$$\bar{M} = \begin{pmatrix} M \\ M \\ \vdots \\ M \end{pmatrix}, \quad \bar{N} = \begin{pmatrix} N \\ N \\ \vdots \\ N \end{pmatrix},$$

$$\bar{L} = \begin{pmatrix} L & & & \\ & L & & \\ & & \ddots & \\ & & & L \end{pmatrix}, \quad U_{max} = \begin{pmatrix} a_{u,max} \\ a_{u,max} \\ \vdots \\ a_{u,max} \end{pmatrix},$$

$$U_{min} = \begin{pmatrix} a_{u,min} \\ a_{u,min} \\ \vdots \\ a_{u,min} \end{pmatrix} \quad (40)$$

The comprehensive indicator equation of the optimization in NMPC is as follows.

$$J = \sum_{i=1}^p [Q_1 \cdot E_m^2(k+i) + Q_2 \cdot (a_{h,lon}(k+i) - a_{ham}(k+1))^2 + Q_3 \cdot (j_{lon}(k+i) - j_{ham}(k+1))^2 + Q_4 \cdot a_u^2(k+i) + Q_5 \cdot \delta^2(k+i) + Q_6 \cdot v_{rlon}^2(k+i)] \quad (41)$$

$$\min\{J\} \quad U(k+m) \quad (42)$$

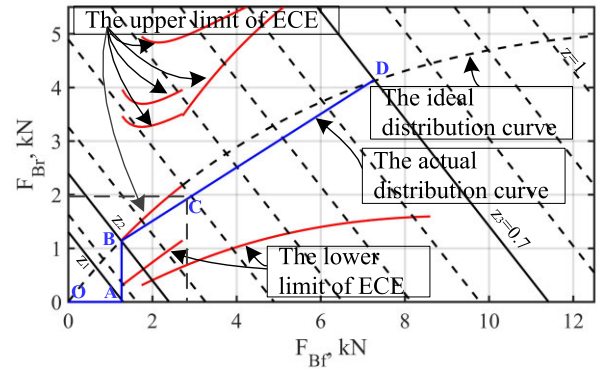


FIGURE 13. Braking force distribution principles in ECE and the braking force distribution strategy.

$$S.t. \Omega \cdot U(k+m) \leq T \quad (43)$$

$$\Omega = \begin{pmatrix} \bar{L}\bar{B} \\ -\bar{L}\bar{B} \\ I \\ -I \end{pmatrix},$$

$$T = \begin{pmatrix} \bar{N} - \bar{L}\bar{A} \cdot x(k) - \bar{L}\bar{G} \cdot W(k+p) \\ -\bar{M} + \bar{L}\bar{A} \cdot x(k) + \bar{L}\bar{G} \cdot W(k+p) \\ U_{max} \\ -U_{min} \end{pmatrix} \quad (44)$$

V. COORDINATED CONTROL STRATEGY

A. OPTIMUM BRAKING FORCE DISTRIBUTION STRATEGY

Given that the participation of Regenerative Braking System (RBS) in EF, the braking force distribution strategy consists of that between front and rear axles and that between the generator and the hydraulic braking system. The RBS aims at recovering the maximum braking energy under constraints of laws and regulations about the braking performance, such as principles in Economic Commission of Europe(ECE). The requirements can be expressed as follows and shown in Figure 13.

$$\left\{ \begin{array}{l} \varpi > \frac{b+z \cdot h_g}{L_w} \\ (0.15 \leq z \leq 0.3) \\ (z-0.08)(b+z \cdot h_g) \leq \varpi \leq \frac{(z+0.08)(b+z \cdot h_g)}{z \cdot L_w} \\ (0.15 \leq z \leq 0.3) \\ \varpi \geq 1 - \frac{(z+0.08)(a-z \cdot h_g)}{z \cdot L_w} \\ (0.15 \leq z \leq 0.3) \\ \varpi \geq 1 - \frac{(z-0.02)(a-z \cdot h_g)}{0.74z \cdot L_w} \\ (0.3 \leq z \leq 0.61) \\ \varpi \leq \frac{(z+0.07)(b+z \cdot h_g)}{0.85z \cdot L_w} \\ (0.2 \leq z \leq 0.80) \\ \varpi \leq 1 - \frac{(z+0.07)(a-z \cdot h_g)}{0.85z \cdot L_w} \\ (0.2 \leq z \leq 0.80) \end{array} \right. \quad (45)$$



where  $\varpi$  is the distribution coefficient of the braking force,  $z$  is the braking strength,  $a$  and  $b$  are distances from the mass center to the front and rear axles respectively,  $h_g$  is the height of the mass center and  $L_w$  is the wheelbase.

The blue line in Figure 10 shows the optimum distribution strategy of braking forces. Distribution strategies in OA and AB segments can be expressed as follows.

$$\begin{cases} OA : F_{gf} = F_b, F_{gr} = 0, F_{Mf} = F_{Mr} = 0, F_b \leq F_{mf} \\ AB : F_{gf} = F_{mf}, F_{gr} = F_b - F_{mf}, F_{Mf} = F_{Mr} = 0, F_{mf} < F_b \leq F_{mf} + F_{mB} \end{cases} \quad (46)$$

where  $F_{Bf}$  is the braking force of the front axle and  $F_{Br}$  is that of the rear axle,  $F_b$  is the desired braking force,  $F_{gf}$  and  $F_{gr}$  are regenerative braking forces of the front and rear axles,  $F_{Mf}$  and  $F_{Mr}$  are hydraulic braking forces of the front and rear axles,  $F_{mf}$  and  $F_{mr}$  are the maximum regenerative braking forces of the front and rear axles,  $F_{mB}$  is the braking force of rear axle in point B.

Generators in front axle recovery maximum regenerative forces as the curve in BC segment and the insufficient part is compensated by those in rear axle and the hydraulic braking system along the BD segment. The distribution threshold is as followed.

$$(F_{mf} + F_{mB}) \leq F_b \leq (F_{mC} + F_{mr}) \quad (47)$$

where  $F_{mC}$  is the braking force of front axle in point C.

Both front and rear generators recovery maximum braking forces as the curve in CD segment and the insufficient part is compensated by those in the hydraulic braking system along the BD segment. The distribution threshold is as followed where  $F_D$  is the braking force in point D.

$$(F_{mC} + F_{mr}) \leq F_b \leq F_D \quad (48)$$

### B. MULTI-MODES SWITCHING STRATEGY

The responding characteristics with shock and delay in M/G causes a frequent mode switching around the braking and driving mode. A finite state machine based mode switching method as shown in Figure 14 and Figure 15. In the first driving exit state, RBS keeps close to avoid the fluctuation of M/G. The regenerative braking force is regained to a certain extent in the second driving state. When it is far away from the driving state in the third stage, the regenerative braking force returns to normal.

The regenerative braking torque of in the M/G decreases to zero gradually from the first stage to the driving mode and can be expressed as follows.

$$T_G = \hat{T}_G - k_1 t, F_{Bri} = -\frac{T_G}{2r_\omega} \quad (49)$$

where  $k_1$  is the reduction rate of M/C torque  $T_G$ ,  $r_\omega$  is the effective rotation radius of the wheel and  $F_{ri}$  is the braking force related to the single wheel. In state NO.2 and NO.3,  $T_G$

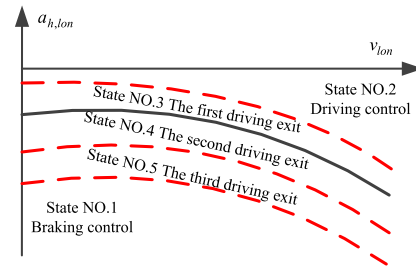


FIGURE 14. Mode switching mechanism between driving and braking control.

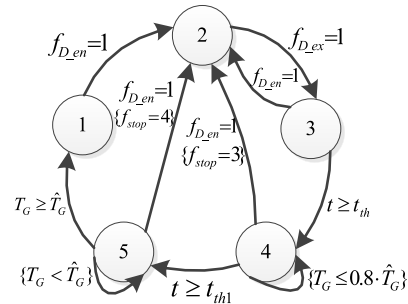


FIGURE 15. Finite state machine of the M/G responding control strategy.

and  $F_r$  are equal to zero and  $T_G$  is 80% of the desired torque in state No.4 and can be expressed as followed.

$$\begin{cases} T_G = \begin{cases} k_2 t & (k_2 t < 0.8 \cdot \hat{T}_G) \\ 0.8 \cdot \hat{T}_G & (k_2 t \geq 0.8 \cdot \hat{T}_G) \end{cases} \\ F_{Bri} = F_{BHri} + \frac{(\hat{T}_G - T_G) \cdot i_0}{2r_\omega} \end{cases} \quad (50)$$

where  $k_2$  is the incremental rate of  $T_G$ ,  $F_{BHri}$  is the hydraulic braking force related to the single wheel. In state NO.5,  $T_G$  is 100% of the desired torque and can be expressed as followed.

$$\begin{cases} T_G = 0.8 \cdot \hat{T}_G + k_2 t \\ F_{Bri} = F_{BHri} + \frac{(\hat{T}_G - T_G) \cdot i_0}{2r_\omega} \end{cases} \quad (51)$$

## VI. EXPERIMENT VERIFICATION AND PERFORMANCE ANALYSIS

### A. EXPERIMENTAL PLATFORM

The co-simulation environment and field test are established for the performance verification of the eco-driving strategy as shown in Figure 16 and Figure 17. Carsim2016<sup>®</sup> achieves a high accuracy vehicle dynamic model for SF and PanoSim-Trunk<sup>®</sup> integrated with the lidar model provides specified scenarios consisting of target vehicles, road and procedures and point clouds of the lidar for IF. Hub motors and battery packs for EF are modeled in Mathworks Simulink<sup>®</sup> as well as the eco-driving strategy for SF. IEV states changes with the procedures and control commands and have an influence on the scenario data with other target vehicles.

Field test platform consists of the multi-modal sensors, the controller and the electric actuators. The eco-driving strategy

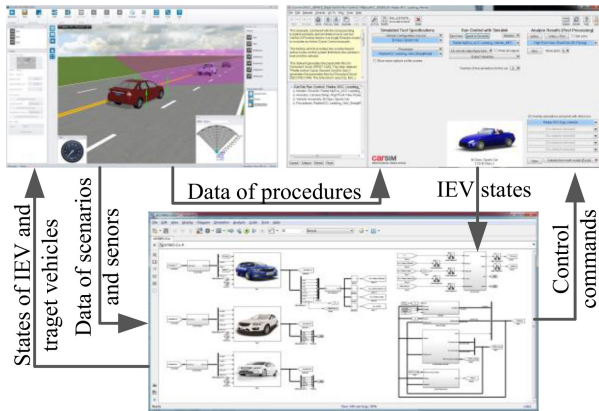


FIGURE 16. The co-simulation environment consisting of PanoSim-Trunk®, Carsim2016® and Mathworks Simulink®.

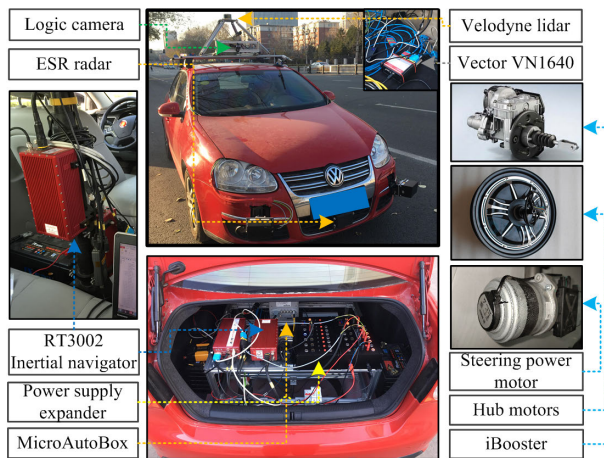


FIGURE 17. The IEV field test platform.

runs on the dSPACE MicroAutoBox. The Velodyne lidar and RT3002 inertial navigator collect data of the point clouds and vehicle states, such as the velocity, acceleration and position. Hub motors, iBooster and the steering power motor system constitute IEV’s actuators. Logic camera, ESR radar and the vector are used to collect raw sensor data for data backup.

Energy recycling efficiency  $\eta_{reg}$  is designed to evaluate the economy performance as follows.

$$\eta_{reg} = \frac{\sum_{m=1}^{p_t} \int_{t_{m-1}}^{t_{m-2}} \frac{T_G \cdot n_G}{9.55} dt}{\sum_{m=1}^{p_t} \frac{1}{2} m_s v_{m-0}^2 - \frac{1}{2} m_s v_{m-1}^2} \quad (52)$$

where  $p_t$  is the braking time interval,  $v_{m-0}$  and  $v_{m-1}$  are the initial and final velocities in the  $m^{th}$  braking,  $t_{m-1}$  and  $t_{m-2}$  are the initial and final moments in the  $m^{th}$  braking,  $m_s$  is IEV’s mass and  $n_G$  is the velocity of the hub motor.

### B. ECO-DRIVING RESULTS IN NORMAL SCENARIOS

The IEV activates Adaptive Cruise Control (ACC) in the normal scenario, aiming at achieving the car-following maneuver

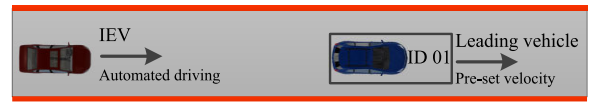


FIGURE 18. The normal scenario specification.

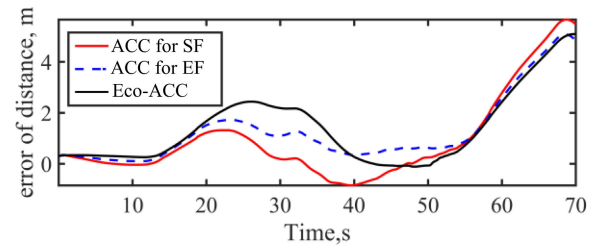


FIGURE 19. Simulation result of the distance following error.

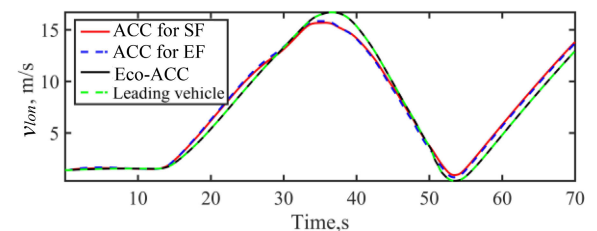


FIGURE 20. Simulation result of the speeds.

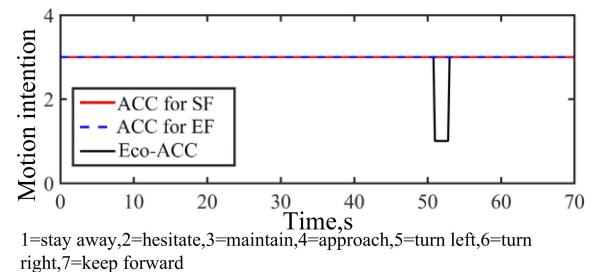


FIGURE 21. Simulation result of the target’s motion intention.

according to the velocity sequences of the leading vehicle, which are pre-set as forms of sine, JP1015, ECE, UDDS and EUDC respectively corresponding to five typical normal scenarios. The Sine-type scenario specification is shown as an example in Figure 18 and simulation results in the normal scenario are shown in Figure.19~Figure.24. The strategy without optimizes comfort indicator is called ACC for EF, and that without optimizes economy and comfort indicators is called ACC for SF.

Simulation results in the sine-type scenarios shows that the tendencies of the distance following error are consistent but a little larger in Eco-ACC mode than the others. IEV velocity follows the leading vehicle well and  $a_{h,lon}$  in Eco-ACC has the minimal difference with that of the human driver but has larger difference with those of the others. The good following and safety performances are obtained in ACC for SF, but with a lower SOC value and fitting goodness of

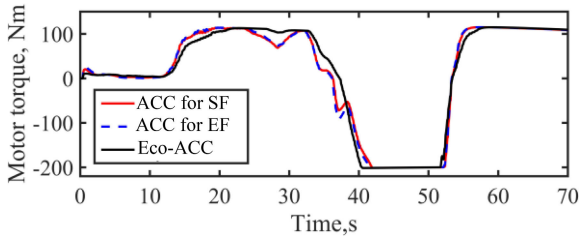


FIGURE 22. Simulation result of the hub motor torques.

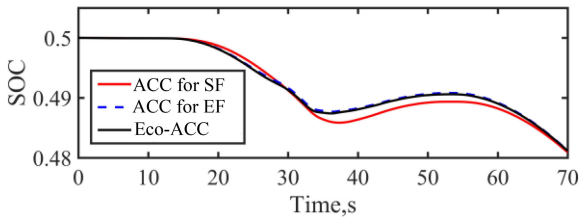


FIGURE 23. Simulation result of the SOC.

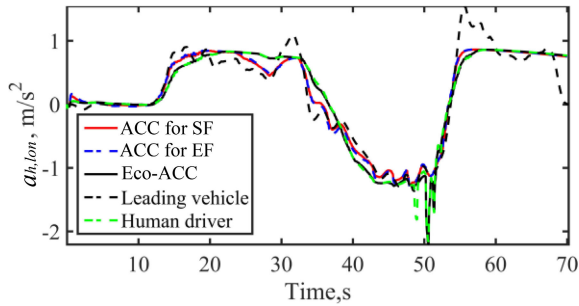


FIGURE 24. Simulation result of the accelerations.

TABLE 1.  $\eta_{reg}$  in typical normal scenarios.

$\eta_{reg}$ , %	Sine	JP1015	ECE	UDDS	NEDC
ACC for SF	31.4	28.6	16.3	34.8	32.5
Eco-ACC	37.3	33.8	20.4	39.9	38.3

$a_{h,lon}$  comparing with that of the human driver. The Eco-ACC strategy has an optimum performance. Consistent optimum results are obtained in other typical scenarios. Corresponding  $\eta_{reg}$  in TABLE 1 shows that the Eco-ACC have stable and better economy performance. Therefore, the Eco-ACC in IEVs improve car-following, safety, economy and comfort performance.

C. ECO-DRIVING RESULTS IN EMERGENCY SCENARIOS

Field test in emergency scenarios with C2C AEB CCRb and LSS test protocols by EuroNCAP are conducted as shown in Figure 25 and Figure 26 respectively. The control authority in IEV is delivered to the active safety controller or the collision avoidance controller, when the situation level is no less than 4. The throttle is taken over and the IEV will brake with the expectation deceleration of  $-0.3g$  in level 4 and  $-0.8g$

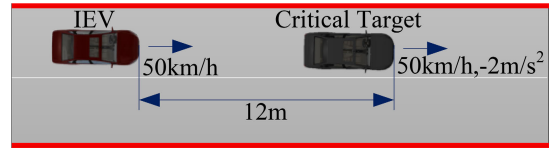


FIGURE 25. The emergency scenario specification CCRb.

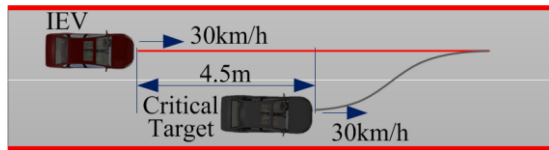


FIGURE 26. The emergency scenario specification LSS.

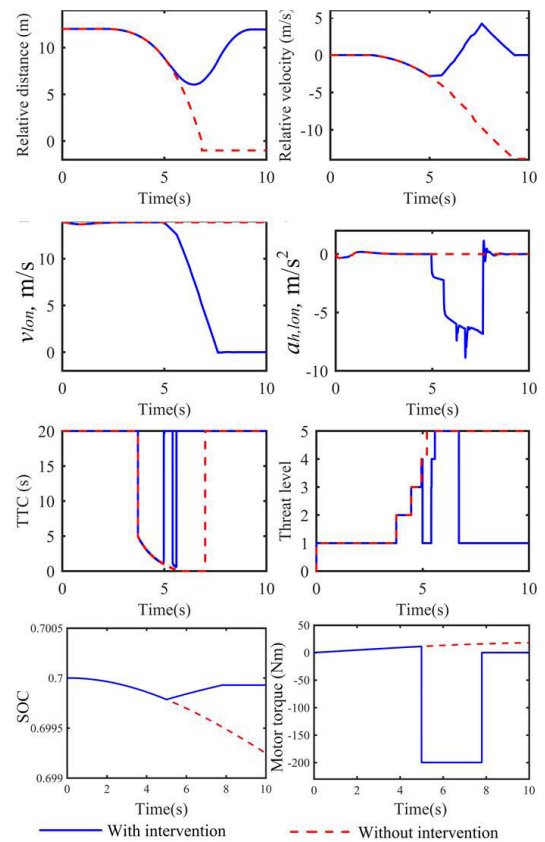


FIGURE 27. Field test results with the EuroNCAP CCRb scenario.

in level 5. Test results with the collision avoidance controller in eco-driving are shown as the examples in Figure 27 and Figure 28 respectively.

As shown in Figure 27 and Figure 28, the collision avoidance controller can detect and track targets with high accuracy and economy. The situation prediction method can conduct correct intervention to avoid collision. The  $\eta_{reg}$  are 6.2% and 5.8% respectively during the collision avoidance process. In the emergency scenarios, the collision avoidance controller can guarantee the safety and improve the economy performance for IEV's eco-driving.

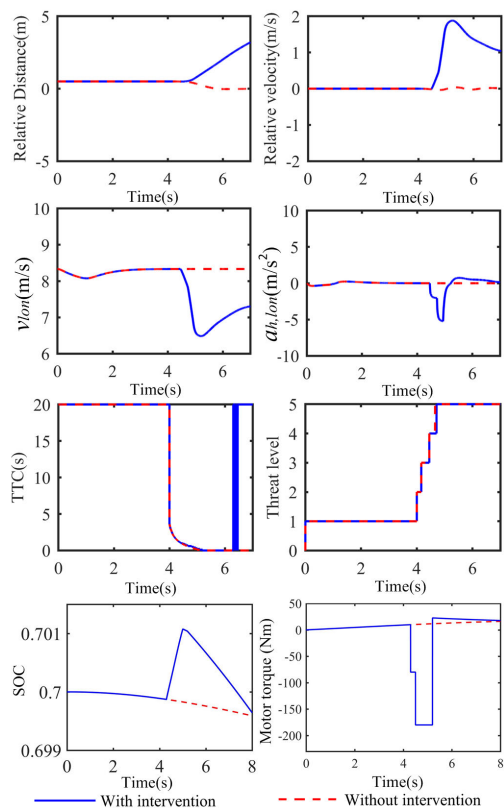


FIGURE 28. Field test results with the EuroNCAP LSS test protocol.

## VII. CONCLUSION AND FUTURE WORK

Given system requirements of IEVs, a coordinated control based longitudinal eco-driving for 4WD intelligent electric vehicles is proposed in this paper. Basing on the theoretical analysis and experiment verification, an intensive intelligent electric vehicle framework basing on the optimal mechanism of energy flow, substance flow and information flow is established. On this basis, an intention-aware longitudinal eco-driving strategy applicable to overall traffic situation levels is developed for the eco-driving strategy. With the coordinated control strategy aiming at arbitrating control modes and distributing braking forces, optimal control effects in overall traffic situation levels and an enhanced energy recycling efficiency have been achieved in the co-simulation environment and field test. The minimum entropy based orderliness structure issue of the SF, EF and IF in time and space will be the future research priority. What's more, the multi-modal sensor fusion basing on lidar and camera will be in-depth study to optimize the effect of scenario situation estimation.

## ACKNOWLEDGMENT

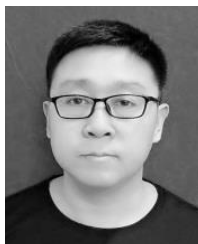
(Dr. Yaxin Li contributed equally to this work).

## REFERENCES

- [1] X. Sun, Z. Li, X. Wang, and C. Li, "Technology development of electric vehicles: A review," *Energies*, vol. 13, no. 1, pp. 1–29, Dec. 2019.
- [2] T. Capuder, D. Zoričić, and H. Pandžić, "Review of challenges and assessment of electric vehicles integration policy goals: Integrated risk analysis approach," *Int. J. Electr. Power Energy Syst.*, vol. 119, pp. 1–12, Jul. 2020.
- [3] Y. Liu, X. Wang, L. Li, S. Cheng, and Z. Chen, "A novel lane change decision-making model of autonomous vehicle based on support vector machine," *IEEE Access*, vol. 7, pp. 26543–26550, 2019.
- [4] X. Ding, Z. Wang, L. Zhang, and C. Wang, "Longitudinal vehicle speed estimation for four-wheel-independently-actuated electric vehicles based on multi-sensor fusion," *IEEE Trans. Veh. Technol.*, vol. 69, no. 11, pp. 12797–12806, Nov. 2020.
- [5] S. Cheng, L. Li, X. Chen, S. Fang, X. Wang, X. Wu, and W. Li, "Longitudinal autonomous driving based on game theory for intelligent hybrid electric vehicles with connectivity," *Appl. Energy*, vol. 268, pp. 1–9, Jun. 2020.
- [6] Y. Li, H. Deng, X. Xu, and W. Wang, "Modelling and testing of in-wheel motor drive intelligent electric vehicles based on co-simulation with Carsim/Simulink," *IET Intell. Transp. Syst.*, vol. 13, no. 1, pp. 115–123, Jan. 2019.
- [7] L. Zhang, Y. Wang, and Z. Wang, "Robust lateral motion control for in-wheel-motor-drive electric vehicles with network induced delays," *IEEE Trans. Veh. Technol.*, vol. 68, no. 11, pp. 10585–10593, Nov. 2019.
- [8] P. Sheng, J. Ma, D. Wang, W. Wang, and M. Elhoseny, "Intelligent trajectory planning model for electric vehicle in unknown environment," *J. Intell. Fuzzy Syst.*, vol. 37, no. 1, pp. 397–407, Jul. 2019.
- [9] M. U. Cuma and T. Koroglu, "A comprehensive review on estimation strategies used in hybrid and battery electric vehicles," *Renew. Sustain. Energy Rev.*, vol. 42, pp. 517–531, Feb. 2015.
- [10] B. Sun, W. Deng, R. He, J. Wu, and Y. Li, "Personalized eco-driving for intelligent electric vehicles," in *Proc. SAE Tech. Paper Ser.*, Aug. 2018, pp. 1–10, doi: 10.4271/2018-01-1625.
- [11] T. Ghandriz, B. Jacobson, L. Laine, and J. Hellgren, "Optimization data on total cost of ownership for conventional and battery electric heavy vehicles driven by humans and by automated driving systems," *Data Brief*, vol. 30, pp. 1–233, Jun. 2020.
- [12] K. V. Singh, H. O. Bansal, and D. Singh, "Feed-forward modeling and real-time implementation of an intelligent fuzzy logic-based energy management strategy in a series-parallel hybrid electric vehicle to improve fuel economy," *Electr. Eng.*, vol. 102, no. 2, pp. 967–987, Jan. 2020.
- [13] L. Xi, X. Zhang, C. Sun, Z. Wang, X. Hou, and J. Zhang, "Intelligent energy management control for extended range electric vehicles based on dynamic programming and neural network," *Energies*, vol. 10, no. 11, pp. 1–18, Nov. 2017.
- [14] Y. He, J. Ma, X. Zhao, R. Song, X. Liu, and L. Wang, "Coordinated stability control strategy for intelligent electric vehicles using vague set theory," *Math. Problems Eng.*, vol. 2020, Art. no. 6793821, Feb. 2020.
- [15] T. Chen, L. Chen, X. Xu, Y. Cai, H. Jiang, and X. Sun, "Estimation of longitudinal force and sideslip angle for intelligent four-wheel independent drive electric vehicles by observer iteration and information fusion," *Sensors*, vol. 18, no. 4, pp. 1–24, Apr. 2018.
- [16] J. Guo, Y. Luo, C. Hu, C. Tao, and K. Li, "Robust combined lane keeping and direct yaw moment control for intelligent electric vehicles with time delay," *Int. J. Automot. Technol.*, vol. 20, no. 2, pp. 289–296, Apr. 2019.
- [17] X. Zhang and X. Zhu, "Autonomous path tracking control of intelligent electric vehicles based on lane detection and optimal preview method," *Expert Syst. Appl.*, vol. 121, pp. 38–48, May 2019.
- [18] C. Lv, X. Hu, A. Sangiovanni-Vincentelli, Y. Li, C. M. Martinez, and D. Cao, "Driving-style-based codesign optimization of an automated electric vehicle: A cyber-physical system approach," *IEEE Trans. Ind. Electron.*, vol. 66, no. 4, pp. 2965–2975, Apr. 2019.
- [19] T. Ando, Y. Zhou, F. Momiyama, K. Aoki, B. Yang, and K. Nakano, "Design of longitudinal controller for automated driving bus," *Int. J. Intell. Transp. Syst. Res.*, vol. 18, no. 3, pp. 436–450, Sep. 2020.
- [20] X. Song, F. Ding, F. Xiao, and D. He, "Data-driven optimal cooperative adaptive cruise control of heterogeneous vehicle platoons with unknown dynamics," *Sci. China Inf. Sci.*, vol. 63, no. 9, pp. 1–12, Sep. 2020.
- [21] Y. Kinosada, T. Kobayashi, and K. Shinohara, "Trusting other vehicles' automatic emergency braking decreases self-protective driving," *Hum Factors*, pp. 1–16, Feb. 2020.
- [22] D. Maggi, R. Romano, and O. Carsten, "Transitions between highly automated and longitudinally assisted driving: The role of the initiator in the fight for authority," *Hum Factors*, vol. 31, Aug. 2020, Art. no. 0018720820946183.
- [23] W. Schwarting, J. Alonso-Mora, and D. Rus, "Planning and decision-making for autonomous vehicles," *Annu. Rev. Control, Robot., Auto. Syst.*, vol. 1, no. 1, pp. 187–210, May 2018.
- [24] Jin, Yin, and Chen, "Advanced estimation techniques for vehicle system dynamic state: A survey," *Sensors*, vol. 19, no. 19, pp. 1–26, Oct. 2019.



- [25] W. Song, G. Xiong, and H. Chen, "Intention-aware autonomous driving decision-making in an uncontrolled intersection," *Math. Problems Eng.*, vol. 2016, Apr. 2016, Art. no. 1025349.
- [26] X. Jin, J. Yang, Y. Li, B. Zhu, J. Wang, and G. Yin, "Online estimation of inertial parameter for lightweight electric vehicle using dual unscented Kalman filter approach," *IET Intell. Transp. Syst.*, vol. 14, no. 5, pp. 412–422, May 2020.
- [27] C. Zhai, F. Luo, and Y. Liu, "A novel predictive energy management strategy for electric vehicles based on velocity prediction," *IEEE Trans. Veh. Technol.*, vol. 69, no. 11, pp. 12559–12569, Nov. 2020.
- [28] C. Zhai, Y. Liu, and F. Luo, "A switched control strategy of heterogeneous vehicle platoon for multiple objectives with state constraints," *IEEE Trans. Intell. Transp. Syst.*, vol. 20, no. 5, pp. 1883–1896, May 2019.
- [29] U. C. Ehlers, E. O. Ryeng, E. McCormack, F. Khan, and S. Ehlers, "Assessing the safety effects of cooperative intelligent transport systems: A bowtie analysis approach," *Accident Anal. Prevention*, vol. 99, pp. 125–141, Feb. 2017.
- [30] X. Zheng, H. Huang, J. Wang, X. Zhao, and Q. Xu, "Behavioral decision-making model of the intelligent vehicle based on driving risk assessment," *Comput.-Aided Civil Infrastruct. Eng.*, vol. 4, pp. 1–18, Oct. 2019.
- [31] Y. Yang, J. Zou, Y. Yang, and D. Qin, "Design and simulation of pressure coordinated control system for hybrid vehicle regenerative braking system," *J. Dyn. Syst., Meas., Control*, vol. 136, no. 5, pp. 1–8, Sep. 2014.
- [32] W. Li, H. Du, and W. Li, "Driver intention based coordinate control of regenerative and plugging braking for electric vehicles with in-wheel PMSMs," *IET Intell. Transp. Syst.*, vol. 12, no. 10, pp. 1300–1311, Dec. 2018.
- [33] C. Zhai, X. Chen, C. Yan, Y. Liu, and H. Li, "Ecological cooperative adaptive cruise control for a heterogeneous platoon of heavy-duty vehicles with time delays," *IEEE Access*, vol. 8, pp. 146208–146219, 2020.
- [34] Y. Yang, Y. He, Z. Yang, C. Fu, and Z. Cong, "Torque coordination control of an electro-hydraulic composite brake system during mode switching based on braking intention," *Energies*, vol. 13, no. 8, pp. 1–19, Apr. 2020.
- [35] X. Pei, H. Pan, Z. Chen, X. Guo, and B. Yang, "Coordinated control strategy of electro-hydraulic braking for energy regeneration," *Control Eng. Pract.*, vol. 96, Mar. 2020, Art. no. 104324.
- [36] L. Zhang, H. Ding, J. Shi, Y. Huang, H. Chen, K. Guo, and Q. Li, "An adaptive backstepping sliding mode controller to improve vehicle maneuverability and stability via torque vectoring control," *IEEE Trans. Veh. Technol.*, vol. 69, no. 3, pp. 2598–2612, Mar. 2020.
- [37] A. H. Ahangarnejad, A. Radmehr, and M. Ahmadian, "A review of vehicle active safety control methods: From antilock brakes to semiautonomy," *J. Vib. Control*, pp. 1–30, Aug. 2020.
- [38] W. Deng, S. Zeng, Q. Zhao, and J. Dai, "Modelling and simulation of sensor-guided autonomous driving," *Int. J. Vehicle Des.*, vol. 56, pp. 341–366, 2011.
- [39] G. Welch and G. Bishop, "An introduction to the Kalman filter," Dept. Comput. Sci., Univ. North Carolina, Chapel Hill, NC, USA, Tech. Rep. TR 95-041, 1995.
- [40] Y. Li, W. Deng, B. Sun, J. Wang, J. Zhao, and B. Zhu, "A maneuver-based threat assessment strategy for collision avoidance," *SAE Int. J. Passenger Cars-Electr. Electr. Syst.*, vol. 12, no. 1, pp. 1–12, Aug. 2019.
- [41] J.-J. Martinez and C. Canudas-de-Wit, "A safe longitudinal control for adaptive cruise control and stop-and-go scenarios," *IEEE Trans. Control Syst. Technol.*, vol. 15, no. 2, pp. 246–258, Mar. 2007.



**LIANG HAO** was born in 1979. He received the B.S. degree in mechanical engineering from Liaoning Technology University, Jinzhou, in 2003, and the M.S. degree in vehicle engineering from Jiangsu University, Zhenjiang, in 2007. He is currently pursuing the Ph.D. degree in vehicle engineering from Shenyang Northeast University, Mechanical Engineering and Automation Academy, Liaoning, China. Since 2007, he has been an Associate Professor of automobile and

traffic engineering academy with Liaoning Technology University. His research interests include system dynamics and control of new energy vehicles and vehicle information fusion technology. His awards and honors include the Liaoning Natural Science Achievement Award, outstanding graduates of Jiangsu University, and advanced individual of Liaoning Technology University.



**BOHUA SUN** was born in 1988. He received the M.S., B.S., and Ph.D. degrees in the automotive engineering academy from Jilin University, Changchun, in 2011, 2014, and 2020, respectively. He participated in the National Science Foundation of China in 2015, the National Key Research and Development Program in 2016, the National Science Foundation of China in 2017, and the National Science Foundation of China in 2018. He won the Second Prize of Science and Technol-

ogy of Jilin province in the project of the braking system in the green vehicle and its testing and matching system in 2019. He has published 21 academic articles, 59 patents, and four software copyrights. His research interests include advanced electronic control, safe and reliable shared control, optimization and integrated control, testing and evaluation techniques of the intelligent vehicle, human-like, and personalized ADAS.



**GANG LI** was born in 1987. He received the B.S. degree in mechanical engineering from National Chung Cheng University, Chiayi, Taiwan, in 2004, and the M.S. degree in mechanical engineering from National Tsinghua University, Taiwan, in 2006. He is currently pursuing the Ph.D. degree in mechanical engineering with Texas A&M university, College Station, TX, USA. Since 2017, he has been a Professor/Master supervisor of vehicle engineering from the Liaoning University of

Technology, Jinzhou, Liaoning. His research interests include drive and control of new energy vehicles and automobile safety and intelligent control. His awards and honors include the 100 Person level candidates of ten million talents project in Liaoning province, the first Prize of the Jinzhou Science and Technology Progress Award and excellent talents in colleges and universities in Liaoning Province.



**LIXIU GUO** was born in 1968. He received the M.S., B.S., and Ph.D. degrees from the Mechanical Engineering and Automation Academy, Northeast University, Shenyang, China, and from Northeast University, Shenyang, in 1994, 1997, and 2004, respectively. Since 2004, he has been a Professor Supervisor of mechanical engineering with Northeastern University. His research interests include vehicle system dynamics and control, finite element analysis of multi physical field coupling, and

mechanical vibration and control. His awards and honors include the 100 Person level candidates of ten million talents project in Liaoning province, winner of new century talents support program of ministry of education, and first prize of the Liaoning Natural Science Academic Achievement Award.

• • •